frontiers | Frontiers in Earth Science

TYPE Original Research
PUBLISHED 21 April 2023
DOI 10.3389/feart.2023.1192997

OPEN ACCESS

EDITED BY
Jiyuan Yin,
Chinese Academy of Geologi-cal Sciences (CAGS), China

REVIEWED BY
Gaoxue Yang,
Chang'an University, China
Xiaoping Long,
Northwest University, China

*CORRESPONDENCE
Xijun Liu,
xijunliu@glut.edu.cn
Hao Wu,
wuhaojlu@126.com

RECEIVED 24 March 2023
ACCEPTED 13 April 2023
PUBLISHED 21 April 2023

CITATION
Tian H, Liu X, Wu H, Li D, Liu X, Song Q, Li Z, Liu P, Hu R and Yang Q (2023), Development of a cambrian back-arc basin in the North Qilian orogenic belt: New constraints from gabbros in Yushigou ophiolite.
Front. Earth Sci. 11:1192997.
doi: 10.3389/feart.2023.1192997

Development of a cambrian back-arc basin in the North Qilian orogenic belt: New constraints from gabbros in Yushigou ophiolite

Hao Tian[1], Xijun Liu[1,2]*, Hao Wu[1,2]*, Dechao Li[1], Xiao Liu[1], Qi Song[1], Zhenglin Li[1], Pengde Liu[1], Rongguo Hu[1,2] and Qijun Yang[1]

[1]Guangxi Key Laboratory of Hidden Metallic Ore Deposits Exploration, College of Earth Sciences, Guilin University of Technology, Guilin, China, [2]Collaborative Innovation Center for Exploration of Nonferrous Metal Deposits and Efficient Utilization of Resource Guilin University of Technology, Guilin, China

Introduction: The North Qilian orogenic belt, as the Northern branch of the original Tethys tectonic domain, is important for reconstructing the tectonic evolution of the ancient Tethys. However, the tectonic history of the North Qilian orogenic belt remains controversial. This study addresses this issue from a geochemical perspective.

Methods: In this study, a comprehensive analysis of the geochronology, whole-rock geochemistry, clinopyroxene mineral geochemistry, zircon Ti crystallization temperature, and gabbromagma temperature and pressure in the Yushigou ophiolite of the North Qilian orogenic belt was conducted to provide constraints on its tectonic evolution.

Results and Discussion: Laser ablation inductively coupled plasma mass spectrometry zircon U-Pb dating results reveal that the gabbros have ages of 519 ± 3 Ma and 495 ± 4 Ma, belonging to the Cambrian period. Most of the studied gabbros exhibited geochemical characteristics of tholeiitic basaltic rocks with normal mid-ocean ridge basalt and island arc tholeiite dual geochemical affinities. The gabbros are interpreted to have formed by a high degree of partial melting of the depleted mantle spinel lherzolite. These results suggest that the back-arc basin of the North Qilian tectonic belt may have evolved to a relatively mature stage from 519 to 495 Ma. Overall, this study contributes to our understanding of the tectonic evolution of the North Qilian orogenic belt through geochemical analyses.

KEYWORDS

mid-ocean ridge basalt, geochemistry, gabbros, back-arc basin, North Qilian

Introduction

Ophiolite fragments of ancient oceanic crust play an irreplaceable role in the identification and reconstruction of ancient oceans, such as their formation and closure, the development of subduction, and the formation of large orogenic belts, and are the most important symbols for identifying converging plate boundaries in collisional and

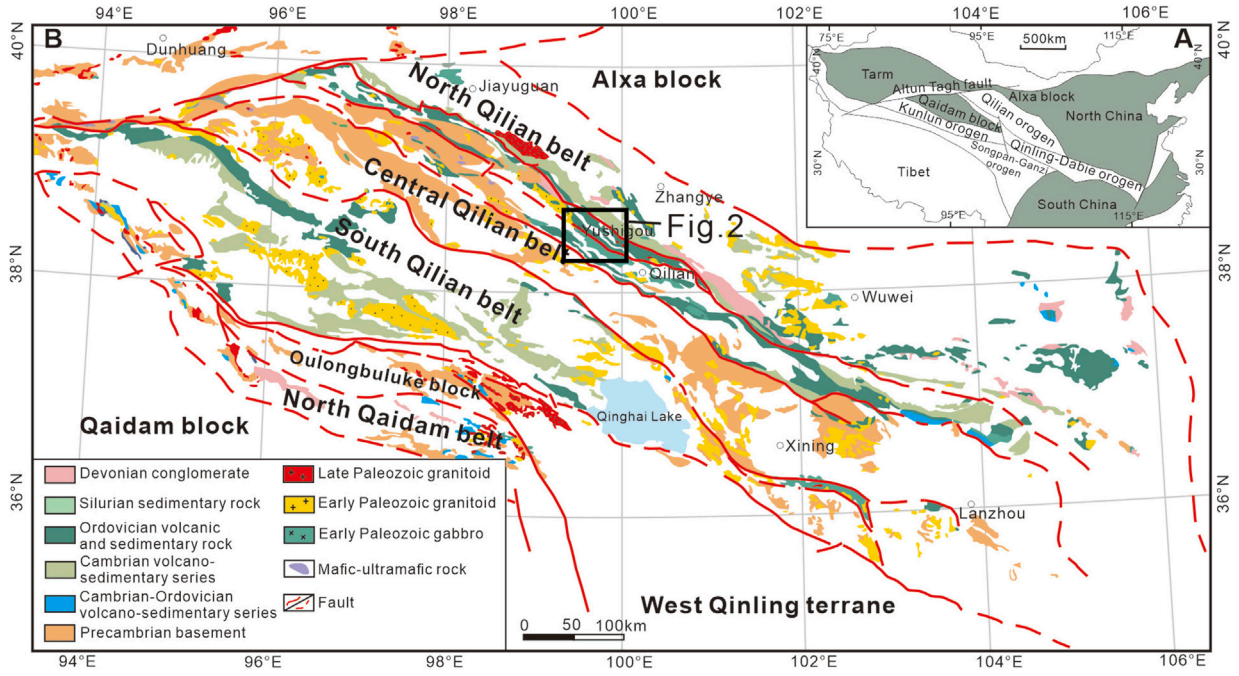

FIGURE 1
(A,B) Geological map of the Qilian orogenic belt (after Fu et al., 2018).

accretionary orogenies (Dilek, 2003; Dilek et al., 2007; Lister and Forster, 2009; Dilek and Furnes, 2011; Song et al., 2015; Wu et al., 2018; Yang et al., 2022).

The North Qilian orogenic belt is a typical Early Paleozoic accretionary orogenic belt. The study of the ophiolite suite in the North Qilian orogenic belt, one of the earliest orogenic belts in China, began in the mid-1970s (Xiao et al., 1978). It is located in central and western China, transecting the boundary of the southern margin of the North China and Qaidam plates between the Alashan Block and the Qilian-Qaidam Micro-Block. The belt stretches E-W for over 1,000 km (Yang et al., 2001). Among the ophiolite suite fragments in the North Qilian orogenic belt, the Yushigou ophiolite has been favored by scholars because of its relatively complete rock assemblage. Scholars began to study ophiolites early; however, ophiolites are complex rock assemblages that involve the interaction between mantle materials and oceanic crust materials, which has always been a difficult point in scientific research (Feng and He, 1995; Zhang et al., 1998; Shi et al., 2004; Tseng et al., 2007; Song et al., 2010).

The most important aspect is the delineation of the ophiolite formation age, which remains controversial (Shi et al., 2004). Previous studies have suggested that the Yushigou ophiolites formed during the Cambrian, Late Cambrian-Early Ordovician, and Precambrian (Xiao et al., 1978; xia et al., 1996; Shi et al., 2004). The tectonic environment of the North Qilian orogenic belt also remains controversial. It is believed to be a mid-ocean ridge, back-arc basin, or subduction environment (Hou et al., 2006; Tseng et al., 2007; Xia et al., 2012; Song et al., 2014). Previous studies on the siliceous rocks in the area suggest that they formed in a continental margin basin or tectonic environment (Du et al., 2006a; b; Zhu and Du, 2007). Previous researchers have also studied the geochemistry of siliceous rocks in the North Qilian orogenic belt and concluded that the tectonic environment of these siliceous rocks, which are associated with volcanic rocks in the rift valley, oceanic crust, island arc, and back-arc basin, was not an oceanic basin or mid-ocean ridge environment, but rather a poly oceanic island or continental margin environment (Du et al., 2007; Yan et al., 2008). In this study, a field geological survey, petrography, zircon U-Pb chronology, and whole-rock geochemistry of the Yushigou ophiolite were conducted in detail. Combined with previously published geological data, the formation age, petrogenesis, and tectonic evolution of the North Qilian orogenic belt were discussed.

Geological background and Petrology

The Qilian orogenic belt (Figure 1A) is part of the Qinling-Qilian-Kunlun fold system (Li et al., 1978), also known as the Central China orogenic belt. It is located in a joint region among the three major blocks in China, namely, the North China Craton in the Northeast, the Yangtze Craton in the southeast, and the Tarim Craton in the northwest (Song et al., 2013a). This study focused on the North Qilian belt and its surrounding areas. At the northeastern margin of the Tibetan Plateau, the North Qilian orogenic belt is an Early Paleozoic suture zone composed of three subunits: the North, Central, and South Qilian belts (Figure 1B; Chen et al., 2014). Furthermore, it is divided into two E-W segments and most ophiolites are distributed in the eastern segment. The ophiolite in the Eastern section of the North Qilian orogenic belt is divided from north to south into the Jiugequan, Dachadaban, Bianmagou, and Yushigou ophiolites.

10.3389/feart.2023.1192997

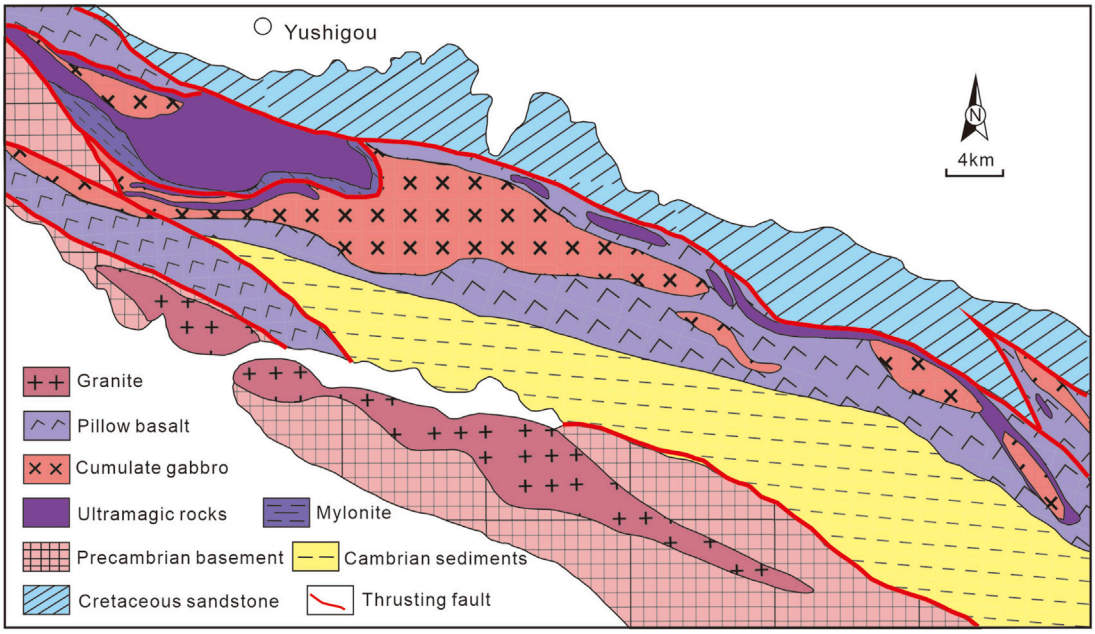

FIGURE 2
Geological map of the Yushigou ophiolite (after Song et al., 2013a).

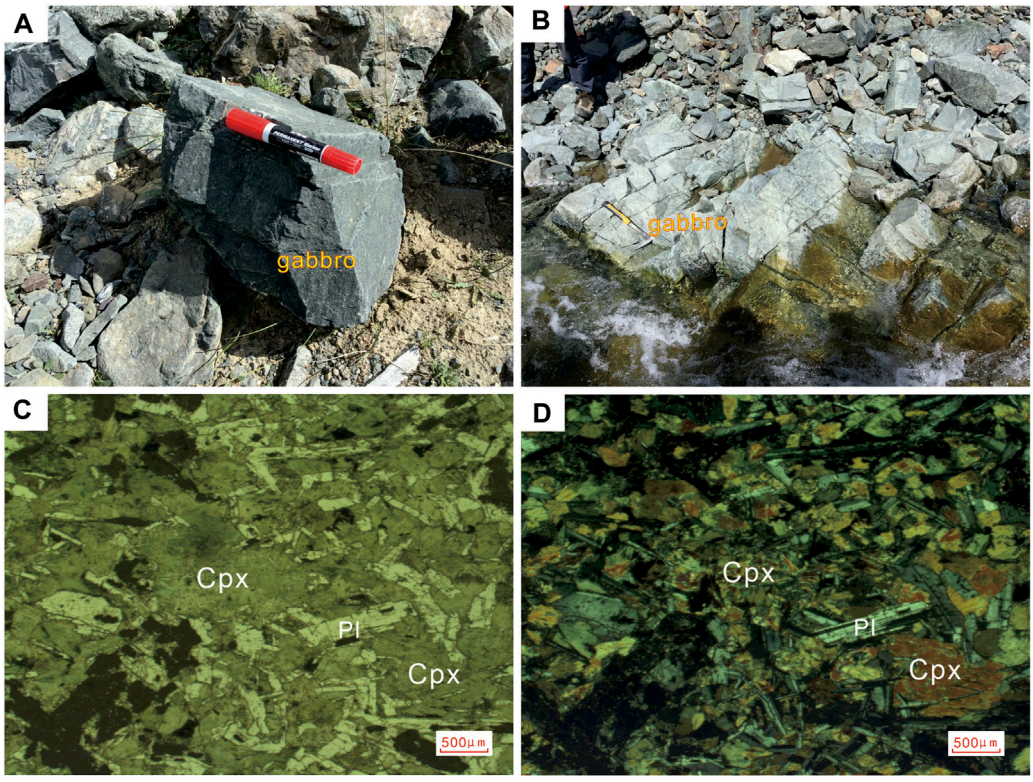

FIGURE 3
(A,B) Field survey photos and **(C,D)** gabbro microscopic photos; Cpx: Clinopyroxene; Pl: Plagioclase.

The Yushigou ophiolite (Figure 2) is found in the middle of the North Qilian belt and represents the boundary between the Alashan Block and the Qilian-Qaidam Micro-Block (Shi et al., 2004; Hou et al., 2006; Song et al., 2013a). The Yushigou ophiolite is 5.0–5.5 km wide from North to South and approximately 14.5 km long from east to west, occurring as a nappe thrust over the Precambrian crystalline basement of the Central Qilian block, in which an ophiolitic mélange appears on both sides (Song et al., 2013a). Carbonatite dykes and carbonated serpentinite blocks are widely observed in the Yushigou mantle complex and have been interpreted as syn-exhumation products formed after serpentinization (Rao, 2015). From North to South, the Yushigou ophiolite consists of peridotites, ultra-mafic to mafic (gabbroic) cumulates, pillow basalts, and sedimentary rocks, including marl and reddish radiolarian chert, in fault contact with each other (Shi et al., 2004; Hou et al., 2006). This set of rock assemblages is an important indicator of the horizontal motion of the plate and represents the remnants of the ancient oceanic crust. In this study, samples from the gabbro in the Yushigou ophiolite were analyzed.

The dominant mineral phase in the Yushigou gabbro is clinopyroxene (40–50 vol%), plagioclase (30–45 vol%), and minor amounts of hornblende (~5 vol%) and olivine (~1 vol%) (Figure 3). The studied gabbro displayed a texture of clinopyroxene and plagioclase reaching 0.5–1 mm in size. A small amount of clinopyroxene exhibited a good euhedral degree. Part of the plagioclase was altered, and another part was gray and translucent under plane-polarized light; the other parts were short, columnar, or plate-shaped.

Analytical methods

Zircon U–Pb geochronology, whole-rock and mineral major and trace element geochemistry, and zircon Hf isotope analyses were conducted at the Guangxi Key Laboratory of Hidden Metallic Ore Deposit Exploration, Guilin University of Technology, China (Zhang et al., 2019; Liu et al., 2020).

Zircon U-Pb dating and Hf isotope

Zircon crystals were extracted from rock samples using conventional crushing, heavy liquid, and magnetic separation techniques and then handpicked. Cathodoluminescence (CL) images of the crystals were used to assess the internal zircon structures and select sites for U–Pb dating. The U–Pb isotopic compositions of the zircons were analyzed using an Agilent 7,500 laser ablation inductively coupled plasma mass spectrometer (LA–ICP–MS). Laser ablation was performed at a constant energy of 80 mJ, with a repetition rate of 6 Hz and spot size of 32 μm. Helium was used to carry the ablated material to the ICP–MS. Elemental corrections were determined relative to the standard glass National Institute of Standards and Technology 610 (Pearce et al., 1997). During our analysis, the Plešovice zircon standard yielded a weighted mean $^{206}Pb/^{238}U$ age of 337.1 ± 0.6 Ma (2σ; mean square weighted deviation (MSWD) = 0.10; n = 52), which is within the error of the suggested value of 337.1 ± 0.4 Ma (Sláma et al., 2008). Age calculations were completed using ICP-MS DataCal (version 8.4; (Liu et al., 2008), and Concordia plots were constructed using Isoplot 3.75 (Ludwig, 2012).

The analyses were performed at a laser beam diameter of 40 μm, repetition rate of 10 Hz, laser power of 100 mJ/pulse, and ablation time of 30 s. GJ-l zircon was analyzed to check the reliability and stability of the instrument. Detailed analytical conditions and procedures were described by Griffin et al. (2000, 2002). Two to four samples were analyzed using the JG-1 standard analyses, and $^{206}Pb/^{207}Pb$ and $^{206}Pb/^{238}U$ values were time-corrected. The raw data were processed offline and reduced using an Excel worksheet (Bühn et al., 2009).

Mineral chemistry

The major elemental compositions of the minerals were measured using a JEOL JXA-8230 electron probe microanalyzer at an accelerating voltage of 15 kV, beam current of 20 nA, and 1–2 μm spot diameter. The dwell time was 10 s for the element peaks and 5 s for the backgrounds adjacent to the peaks. Data were reduced using the atomic number absorption fluorescence correction procedure. The trace elements in the Yushigou clinopyroxene were determined using LA-ICP-MS. The analysis was performed using an Agilent 7500cx ICP-MS and an NWR-193 excimer LA system from Elementary Scientific Company. To determine the clinopyroxene content, we used helium as the carrier gas, and each analysis was performed at 8 Hz, 4 J/cm^2 energy, 30 μm spot diameter, over 40 s. Standard reference glasses SRM 610, SRM 612, and BCR-2G were used as external standards to correct the mass discrimination and time-dependent drift. The analytical accuracy and precision of major and trace elements were better than 10%.

Major and trace element analyses

Fresh samples were collected and crushed, and the chips were soaked in 4 N hydrochloric acid for 30 min to remove any altered material. Rock chips were powdered using an alumina ceramic shatterbox. Prior to major element analyses, loss-on-ignition values were measured using a muffle furnace at a constant temperature of 1,000°C. The baked samples were then formed into glass disks with $Na_2B_4O_7$ $10H_2O$ at 1,150°C. ZSX Primus II X-ray fluorescence was used to determine the composition of major elements. The trace element compositions were measured using an Agilent 7500cx ICP-MS. The precision of the major and trace element measurements was 2%–5%. Standardization was performed using United States Geological Survey (USGS) standards BHVO, AGV, W-2, and G-2 and national rock standards GSR-1, GSR-2, and GSR-3 (Zhang et al., 2019).

Analytical results

Zircon U-Pb geochronology and Lu-Hf isotope

The Zircon U-Pb dating results are listed in Supplementary Table S1. The zircons are mostly euhedral and reveal long to short prismatic forms, with average crystal lengths of 150–300 μm and length-to-width ratios from 2:1 to 3:1. Most zircons were

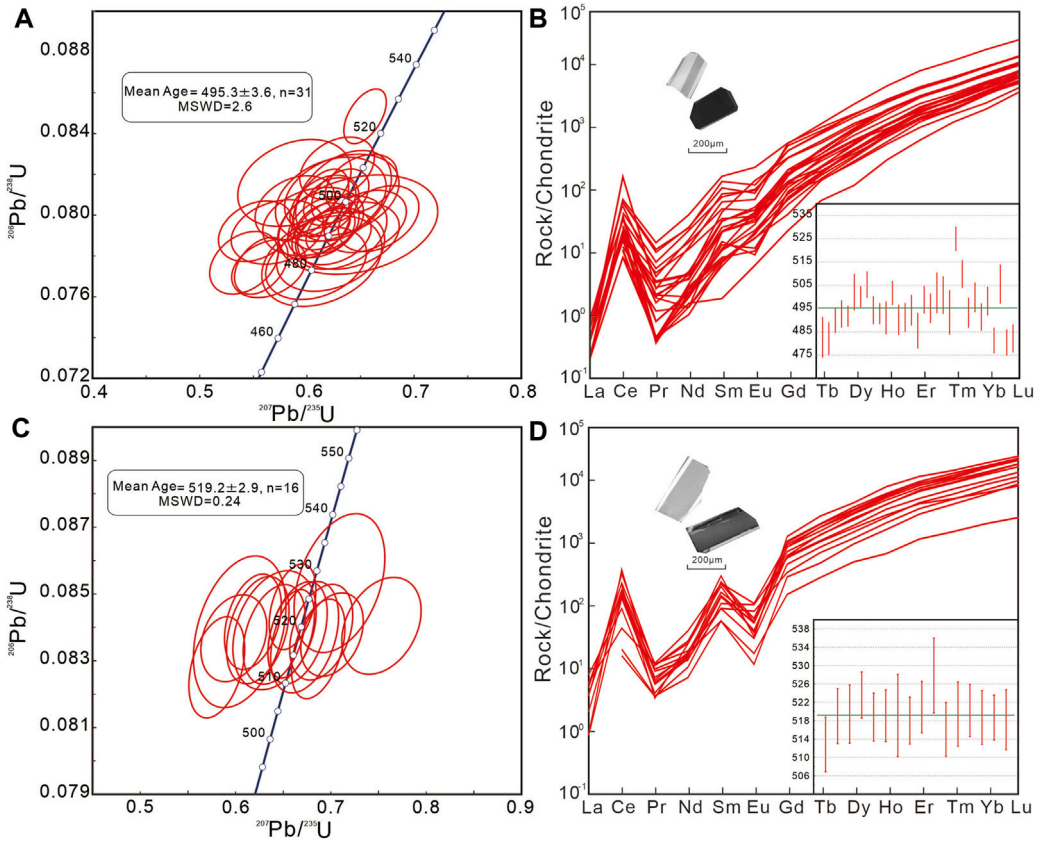

FIGURE 4
(A,C) U-Pb Concordia diagram, weighted mean ages, and mean square weighted deviation (MSWD); **(B,D)** chondrite-normalized rare Earth element (REE) patterns and cathodoluminescence (CL) images for zircons from the Yushigou gabbro. Normalizing values are from Sun and McDonough (1989).

transparent and colorless or pale brown. In the CL images, the zircon crystals are internally homogeneous with weak, broad zoning and without complex internal structures, as is typical of zircons formed in gabbroic magmas (Corfu et al., 2003). All zircon rare Earth element (REE) partition curves show depletion of light rare Earth elements (LREE) and enrichment of heavy rare Earth elements (HREE), with positive Ce anomalies and negative Pr and Eu anomalies. In addition, no overgrowths, mineral or fluid inclusions, or metamictization were observed in the analyzed zircons, suggesting that the zircons were not affected by post-magmatic processes. Thus, the interpretation of the zircon U-Pb isotopic results is simple (Figure 4), and the obtained ages represent the formation time of the gabbro. The Th/U value of the analyzed spots varies from 0.31 to 2.72, suggesting the zircons are of magmatic origin (Williams, 2001; Rubatto, 2002). U-Pb isotopic analyses yielded disparate zircon $^{206}Pb/^{238}U$ ages of 495.3 ± 3.6 Ma (mean square weighted deviation (MSWD) = 2.6) and 519.2 ± 2.9 Ma (MSWD = 0.24), respectively.

The Lu-Hf isotopes were analyzed on selected zircon grains from two different samples that were previously systematically analyzed with U-Pb. Lu-Hf analysis was performed on 41 representative zircon grains dated using the LA-ICP-MS U-Pb method. The results are shown in Supplementary Table S2. The initial Hf composition of zircon represents the $^{176}Hf/^{177}Hf$ value calculated at the time of zircon crystallization, namely, the U-Pb age, likely concordant with that previously obtained for the same crystal. The two-stage depleted mantle Hf model ages (T_{DM} Hf) were calculated using $^{176}Lu/^{177}Hf = 0.0384$ and $^{176}Hf/^{177}Hf = 0.28325$ for the depleted mantle (Chauvel and Blichert-Toft, 2001). The resulting $^{176}Lu/^{177}Hf$ values ranged from 0.282,809 to 0.282,973 with a mean of 0.282,877, indicating that the zircons were weak in radiogenic Hf. The initial zircon $^{176}Hf/^{177}Hf$ value varies with age. Zircons from sample 21-YSG335 had a high $\varepsilon_{Hf}(t)$ between +6.54 and +17.34, with an average of 14.28. The T_{DM} values were restricted to the narrow range from 0.41 to 0.86 Ga. Zircons from sample 21-YSG341 were characterized by positive $\varepsilon_{Hf}(t)$, ranging between +12.13 and +15.8, and T_{DM} values ranging between 0.44 and 0.67 Ga. Their $\varepsilon_{Hf}(t)$ values were close to that of the depleted mantle evolution curve, suggesting that these zircons crystallized from magma with a juvenile signature.

Geochemistry of the major elements

Supplementary Table S3 shows that the SiO_2 contents of the 12 samples range from 45.40 wt% to 57.20 wt%, and the rocks are characterized by low TiO_2 (0.24–1.78 wt%), K_2O (0.01–0.57 wt%) and high Na_2O (0.45–5.15 wt%) contents. The high loss of ignition of rocks (1.62–6.03 wt%) indicates that the samples are slightly altered. The K_2O and Na_2O contents of the rocks may be related to alteration by K- and Na-rich fluids (such as seawater) after

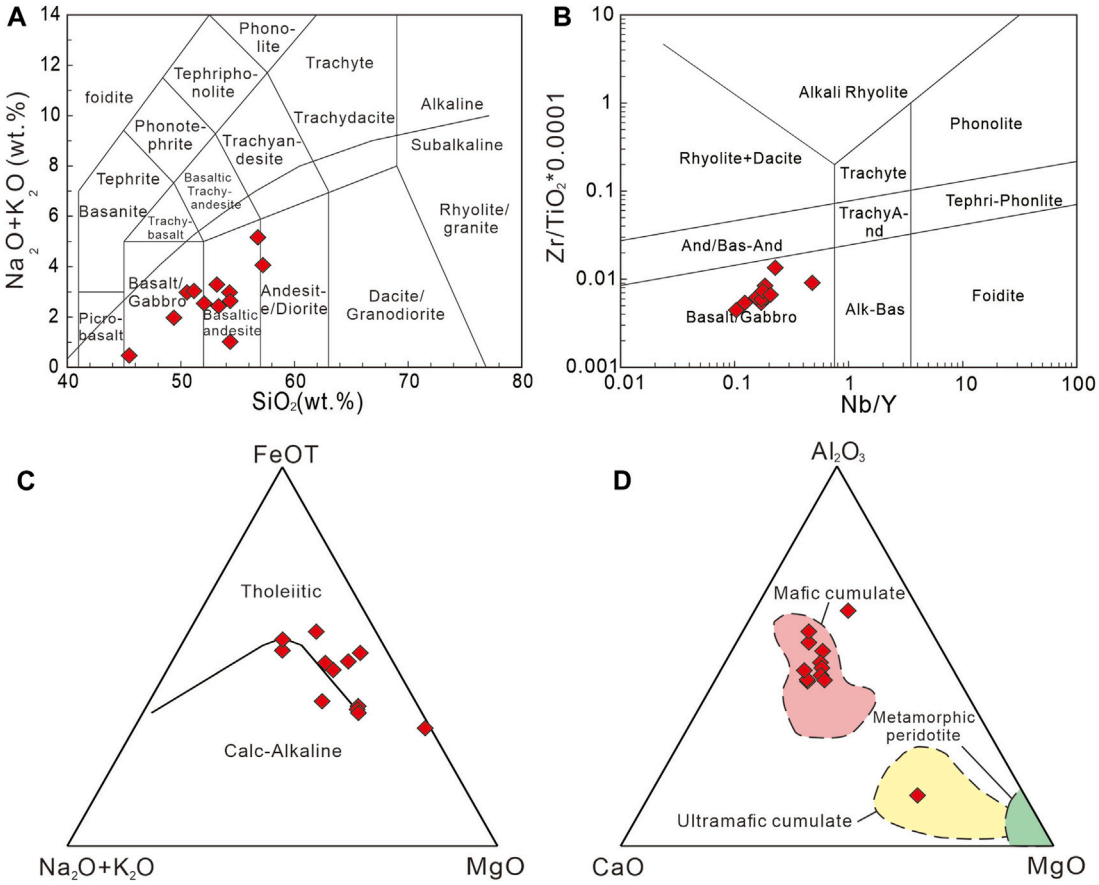

FIGURE 5
(A) Total alkali silica diagram (Le Bas et al., 1986); **(B)** Zr/TiO_2*0.0001-Nb/Y diagram (after Pearce, 1996); **(C)** Al_2O_3-FeOT-MgO composition diagram; and **(D)** Al_2O_3-CaO-MgO composition diagram (Coleman R G, 1977).

formation. The gabbros are enriched in MgO (4.09–25.22 wt%), $Mg^{\#}$ (46.9–82.0), and CaO (3.95–12.92 wt%). This reflects the combined plagioclase and clinopyroxene compositions of the initially formed basic rocks.

The samples collected in this study were greyish-black with medium-to coarse-grained structures. They were mainly composed of clinopyroxene and plagioclase in nearly equal amounts. The secondary mineral is amphibole, which contains small amounts of quartz. Under a single polarized electron microscope, the entire thin section of the sample was dark green, showing a gabbro structure, and the contents of clinopyroxene and feldspar were almost equal. Field and electron microscope observations indicated that the samples collected were gabbro. The results shown in the total alkali-silica diagram are consistent with field observations and electron microscopy (Figure 5A). As the samples were likely altered by K- and Na-rich fluids, the increase in the total alkali content and loss of ignition caused a shift in the rock composition. To further determine the rock type, immobile high-field-strength elements were used for discrimination (Figure 5B), showing that all samples fell into the basalt field. Regarding the relationship between FeO^T, MgO, and Na_2O+K_2O (Figure 5C), most of the rocks were of the tholeiitic series, and the rest were of the calc-alkaline series. In the Al_2O_3-CaO-MgO diagram (Figure 5D), almost all samples were distributed within the mafic cumulative rock fields, and one of the samples fell within the ultramafic cumulative rock fields.

Rare earth elements and trace element geochemistry

Yushigou gabbros have low ΣREE content ranging from 8.36 to 75.60 ppm, with low to slight enrichment in LREE in the chondrite-normalized REE distribution patterns (Figure 6A). The $(La/Yb)_N$ values range from 0.80 to 1.66, while the $(La/Sm)_N$ values vary from 0.54 to 1.61. The parallel REE distribution lines indicate that all samples were derived from the same magma source. In addition, the gabbro samples displayed mid-ocean ridge basalt (MORB)-like trace-element characteristics. Notably, two samples exhibited Nb and Ta depletion (Figure 6B).

Clinopyroxene characteristics

The major and trace element data for clinopyroxenes in the Yushigou gabbro are presented in Supplementary Tables S4, S5. The analyzed clinopyroxene grains from the Yushigou gabbro were augmented (Figure 7A). Clinopyroxene analysis of the Yushigou gabbro showed relatively high MgO (14.28–16.09 wt%) contents, with Mg# (100 × Mg/[Mg + Fe^{2+}]) values ranging from 61 to 65. The grains are characterized by relatively low Al_2O_3 (3.46–8.61 wt

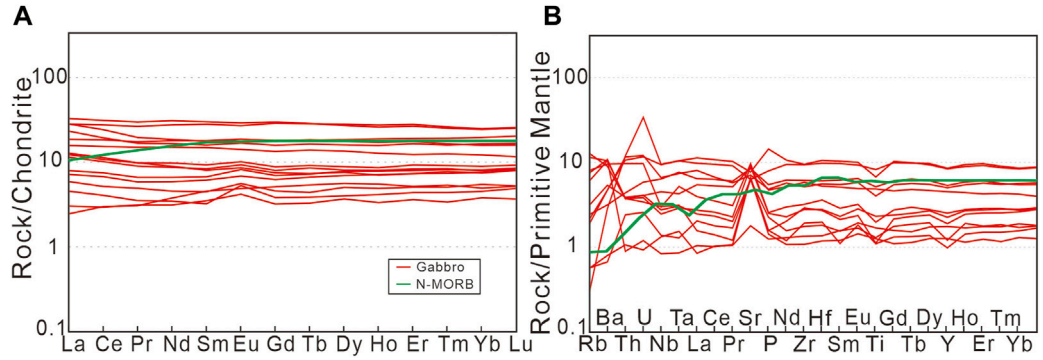

FIGURE 6
(A) Chondrite-normalized REEs; **(B)** Primitive-mantle-normalized trace elements. Normalization values are from Sun and McDonough (1989); N-MORB, normal mid-ocean ridge basalt.

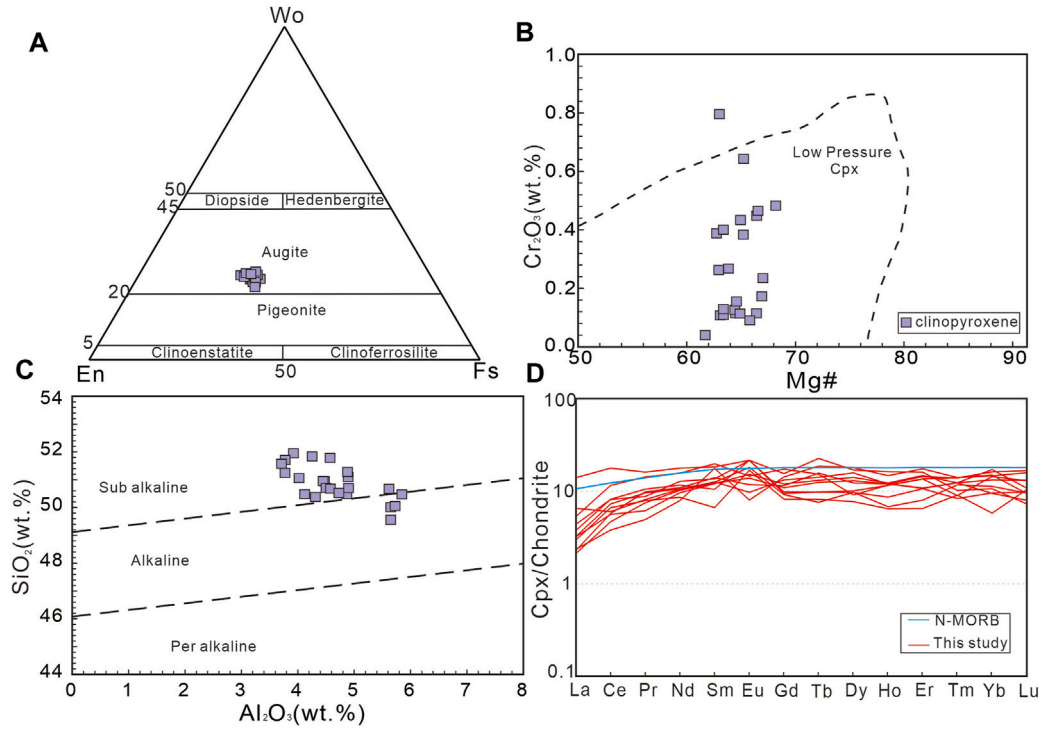

FIGURE 7
Clinopyroxene compositions diagrams; **(A)** Wo-En-Fs diagram modified after Mahoney et al. (1998); **(B)** Cr_2O_3 vs. Mg# in clinopyroxenes (Elthon, 1987), **(C)** SiO_2 vs. Al_2O_3 diagram (after Le Bas, 1962), and **(D)** Chondrite-normalized REEs. Normalization values are from Sun and McDonough. (1989).

%) and Na_2O (0.40–1.18 wt%) contents and high Cr_2O_3 (0.27–2.37 wt%) content. These results suggest that the clinopyroxenes of the Yushigou gabbro were subalkaline and crystallized under medium- and low-pressure conditions (Figures 7B, C). The clinopyroxenes exhibit low total REE contents (9.49–38.36 ppm). The REEs in the Yushigou clinopyroxene samples had characteristics of normal (N-)MORB with a relatively flat trend (Figure 7D). Compared to HREEs, LREEs were slightly depleted.

Discussion

Formation age

Based on previous studies of the North Qilian orogenic belt, we collected the ages of the ophiolites in Yushigou and adjacent areas, which can be divided into three major stages according to their formation time. The first stage occurred at ~550 Ma, and its lithology was mainly composed of gabbro (566–516 Ma),

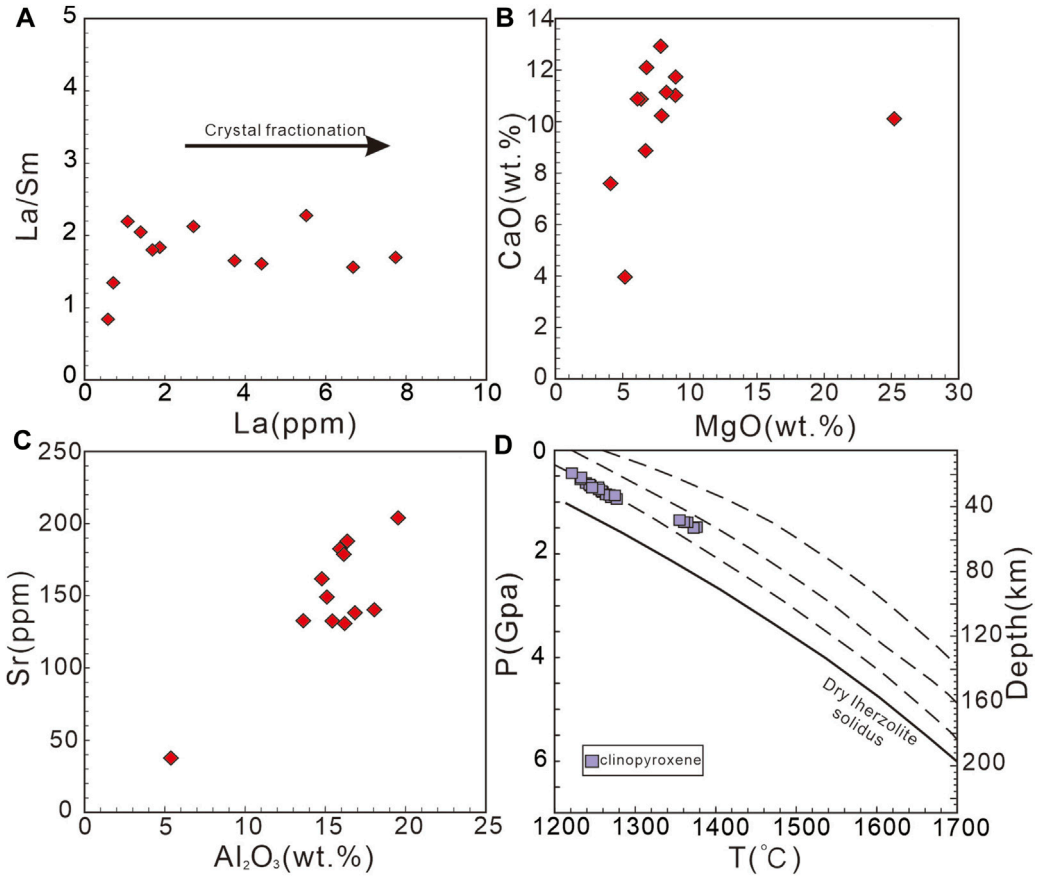

FIGURE 8
(A) La/Sm vs. La diagram; **(B)** CaO (wt%) vs. MgO (wt%) diagram; **(C)** Sr (ppm) vs. Al_2O_3 (wt%) diagram; **(D)** Relationship between temperature, pressure, and depth (Lee et al., 2009).

volcanic rock (593 Ma), amphibolite (534 Ma), and a subduction complex (545 Ma) (Xia et al., 1995; Shi et al., 2004; Song et al., 2019; Yan et al., 2019). The second stage was from 520 to 490 Ma; the lithology of this stage was mainly volcanic rock (495 Ma), gabbro (513–490 Ma), and ophiolites (504–495 Ma) (Xia et al., 1995; Xiang et al., 2007; Zeng et al., 2007; Xia and Song, 2010; Song et al., 2019). The third stage occurred at ~450 Ma, and its main lithology was gabbro (479–448 Ma) (Song et al., 2007; 2013a).

Shi et al. (2004) found that the complementarity between cumulative gabbro and lharzolite in the Yushigou ophiolite was stronger than that between the upper pillow lava and lharzolite, indicating that gabbro represents the melting products of the primitive mantle during the formation of the Yushigou ophiolite. Based on this, zircon U-Pb dating of two gabbro samples from the Yushigou ophiolite was conducted, showing weighted mean ages of 495.3 ± 3.6 Ma and 519.2 ± 2.9 Ma, respectively. This indicates that they formed during the second stage (520–490 Ma). Combined with the results of previous studies and our age determination, we suggest that the ophiolite in the North Qilian belt first formed in the Cambrian period.

Petrogenesis

Magmatic evolution

For a basic–ultrabasic rock series resulting from separation crystallization, the projection points on the La/Sm vs. La elemental covariant map form a horizontal line (Allegre and Minster, 1978; Yang and Gu, 1990). In the La/Sm-La diagram (Figure 8A), the horizontal and linear relationship indicates that separation crystallization is the main factor controlling magma evolution rather than partial melting. The general trends of CaO and MgO in the Yushiguo gabbros indicated significant fractionation of olivine and clinopyroxene (Figure 8B). Moreover, the increase in Sr content with increasing Al_2O_3 content (Figure 8C) suggests the removal of plagioclase. However, the Yushigou gabbros do not show a significant negative Eu anomaly, indicating that plagioclase may not have been significantly fractionated during magma evolution.

Temperature is a key variable controlling magmatic phase equilibria (Neave and Putirka, 2017). In addition to composition, crystallinity, and oxygen fugacity, pressure is another primary variable that affects magmatic phase equilibria (Yoder and Tilley, 1962). Understanding the distribution of the magma storage depth within the lithosphere provides information on both

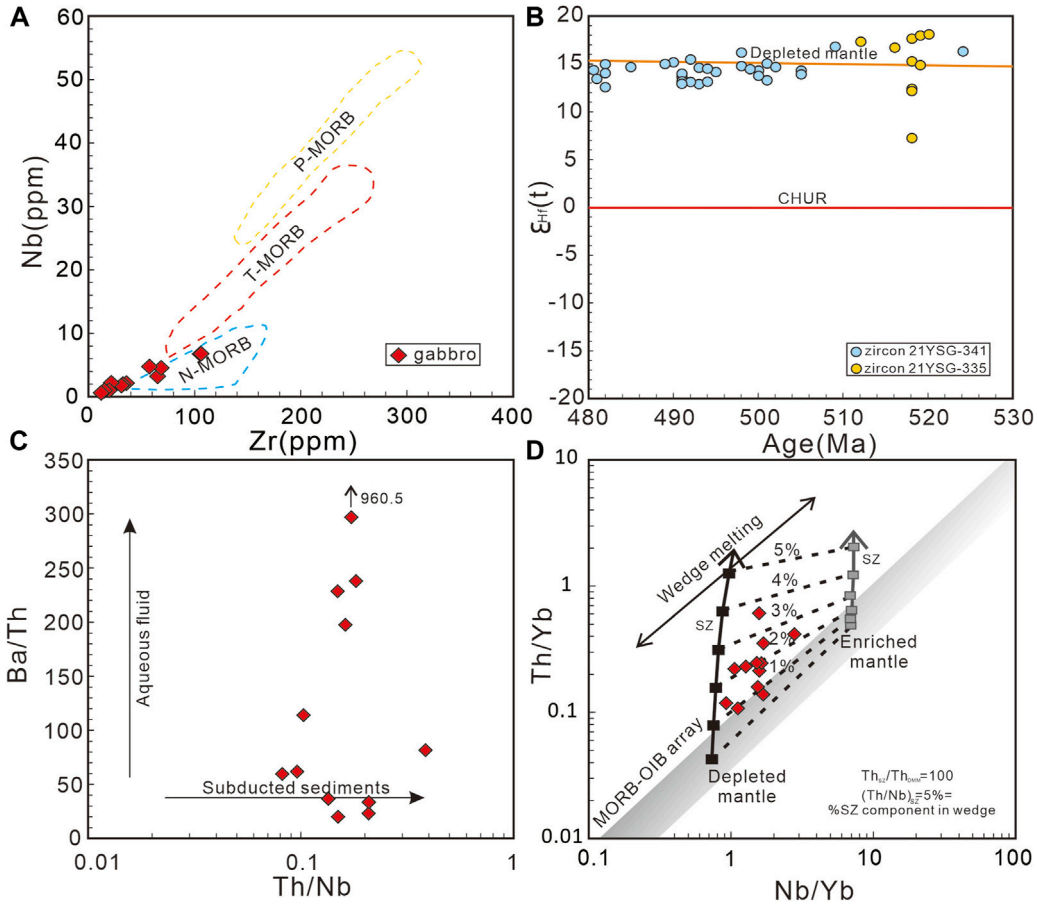

FIGURE 9
(A) Nb vs. Zr diagram (Le Roex et al., 1983); **(B)** $\varepsilon_{Hf}(t)$ vs. Age diagram (Matteini et al., 2010); **(C)** Ba/Th vs. Th/Nb diagram; **(D)** Th/Yb vs. Nb/Yb diagram (after Pearce, 2008); N-MORB, normal or depleted mid-ocean basalt ridge; T-MORB, transitional MORB; P-MORB, plume enriched MORB; CHUR, chondritic uniform reservoir.

oceanic and continental crustal formation mechanisms (Henstock et al., 1993; Kelemen et al., 1997; Annen et al., 2006). Therefore, it is essential to determine magma storage pressures and depths.

In this study, the clinopyroxene thermometer proposed by Putirka (2008) was used to calculate the temperature and pressure of the gabbro in the Yushigou ophiolite. The formation temperature of clinopyroxene is 1,221.3°C–1,376.6°C, and the pressure at this temperature is 4.5–15.0 kbar. The temperature range of the Yushigou ophiolite was 1,174°C–1,402°C, and the mineral phase equilibrium temperature was approximately 1,230°C, which is consistent with the temperature measured in this study. The consolidation equilibrium temperature of mantle magmatic rocks in the Yushigou ophiolite is speculated to be approximately 1,200°C (Yan, 2014). In this study, temperature, pressure, and depth models (Lee et al., 2009) were used to estimate the mantle magmatic depth of the Yushigou ophiolite. The simulation estimated the depth of the clinopyroxene crystals, indicating that the mantle magmatic rocks in the Yushigou ophiolite began to consolidate at approximately 60 km (Figure 8D).

Magma source

The Yushigou gabbro is a magmatic rock of the tholeiitic series, featuring mild large-ion lithophile elements and high-field strength elements, which are typical geochemical characteristics of MORB. The geochemical characteristics of the trace elements show that the gabbro formed in the depleted mantle. The rare Earth distribution curve and trace element multi-element diagram of the Yushigou gabbro are nearly parallel to those of N-MORB (Figure 6), and the Th/Ta, Th/Yb, and Zr/Nb values of trace elements in the Yushigou gabbros are similar to those of the depleted mantle (Th/Ta=2.2, Th/Yb=0.25, Zr/Nb=18, from Condie (1989)). As shown in the Nb vs. Zr diagrams (Figure 9A), the Yushigou gabbros fall near the primitive mantle line, which is close to the depletion type. In addition, the Hf isotopes of the zircons reflect the characteristics of the source area. No inherited or captured zircon was found in the gabbro-zircon CL image or *in situ* micro-survey of the Yushigou ophiolite, indicating that the zircon crystallized in a homogeneous, unmixed magmatic source. The relatively high $\varepsilon_{Hf}(t)$ values of the Yushigou gabbros indicate that they primarily originated from depleted mantle (Figure 9B).

Ba is a fluid-active element (Kessel et al., 2005), which easily enters the mantle *via* fluid migration during subduction (Morris and

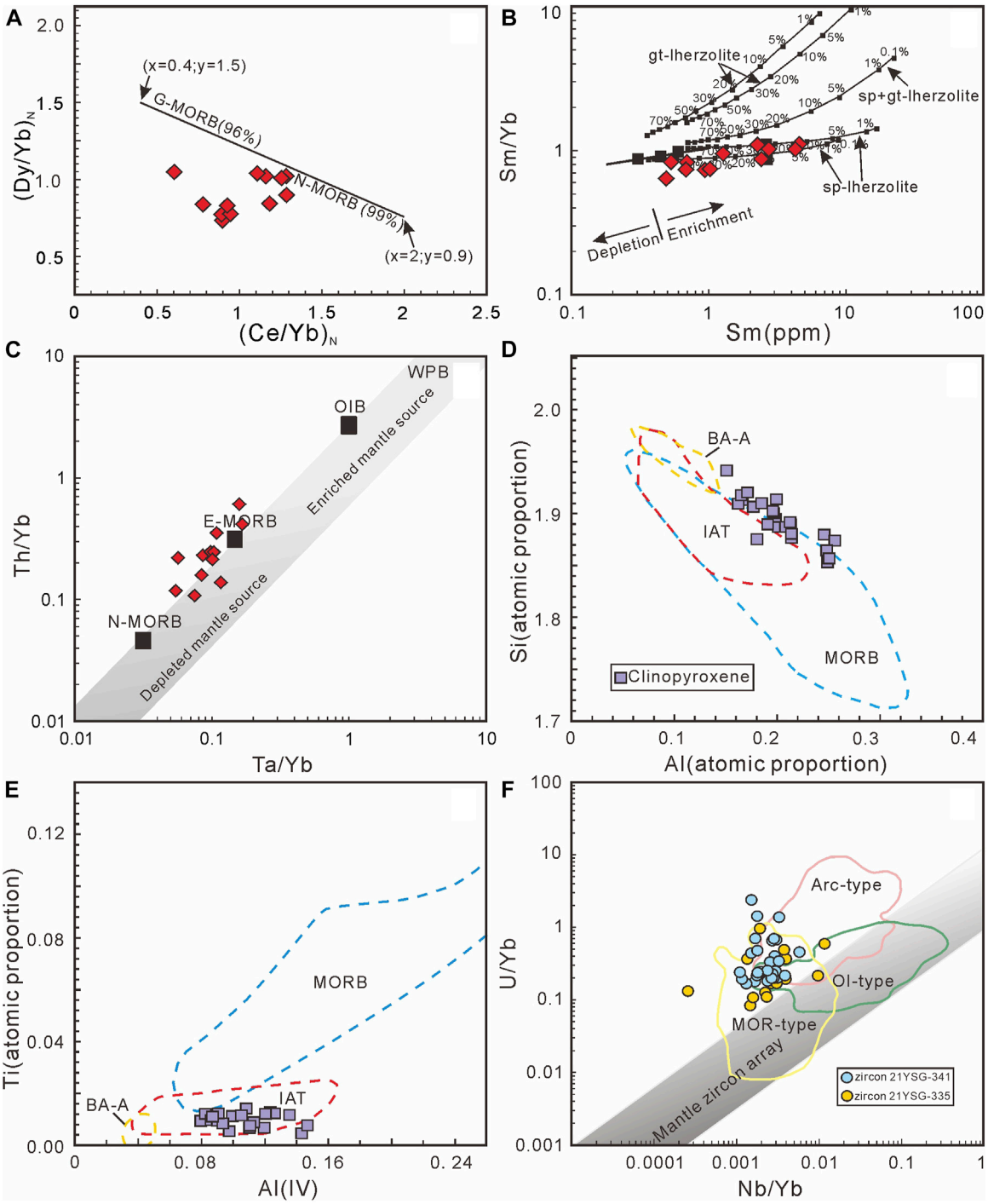

FIGURE 10
(A) $(Dy/Yb)_N$ vs. $(Ce/Yb)_N$ diagram (Saccani, 2015); **(B)** Sm/Yb vs. Sm diagram (Aldanmaz et al., 2000); **(C)** Th/Yb vs. Ta/Yb diagram (Pearce, 1982); **(D)** Si vs. Al diagram; **(E)** Ti vs. Al (IV) diagrams (Beccaluva et al., 1989) of clinopyroxene composition (atomic proportion); and **(F)** Zircon U/Yb vs. Nb/Yb diagram (Grimes et al., 2015);. OI, ocean-island; MOR, mid-ocean ridge; MORB, mid-ocean ridge basalt.; G-MORB, garnet source basalts; N-MORB, normal mid-ocean basalt ridge; Arc, continental arc; BA-A, back-arc andesite; IAT, island-arc tholeiite.

Ryan, 2003). Because of the significant difference in the Ba content between the crust and mantle, Ba can be used to trace the recirculation-related processes of subducting materials (Elliott et al., 1997; Murphy et al., 2002; Pearce and Stern, 2006; Kuritani et al., 2011). A high Ba/Th value indicates aqueous fluid from the dehydrated ocean crust or sediment, and a high Th/Nb value indicates the addition of partially melted material from subducted sediments. The studied samples showed high Ba/Th and Th/Nb values, indicating that they were affected by two subduction components (Figure 9C), and the additional

subduction components comprised 1%–3% of the total composition (Figure 9D).

Recent research has shown that, in contrast to N-MORB, garnet source basalts (G-MORB) exhibit a significant garnet signature (e.g., Montanini et al., 2008; Saccani et al., 2008; 2013). This garnet signature can be highlighted using LREE/HREE and middle rare Earth elements (MREE) to HREE ratios, such as Ce/Yb and Dy/Yb. In the chondrite-standardized $(Ce/Yb)_N$ vs. $(Dy/Yb)_N$ diagram, all sample sites are located on the N-MORB side (Figure 10A), which is significantly different from the G-MORB and depleted of HREE. This indicates that the Yushigou gabbro was derived from a mantle source of non-garnet peridotite (Saccani, 2015). The Ce/Yb values of gabbros ranged from 2.18 to 4.63, which indicates that the gabbros were sourced from the stable zone of spinel less than 70 km deep (Xiao et al., 2003). This is consistent with the formation depth of clinopyroxene in the simulation, where spinel lherzolite partial melts, mantle residues, and melts have similar Sm/Yb values, and Sm values decrease with an increase in the partial melting degree (Aldanmaz et al., 2000). Therefore, the Yushigou gabbro falls within the spinel lherzolite region, and the Sm values vary widely, whereas the Sm/Yb values are relatively constant (Figure 10B).

Geodynamic interpretations

Active elements (Cs, Rb, Sr, and Na) migrate under the influence of alteration and are not effective indicators of tectonic environments; however, most high-field elements (Ta, Nb, Zr, Hf, Ti, Th, and REE) are unaffected (Mullen, 1983). In this study, high-field elements were used to identify the tectonic environment of the Yushigou ophiolite suite gabbro. Studies have demonstrated that both Th and Ta are closely related to subduction. Both are highly incompatible elements, and their elemental ratios remain relatively stable during mantle melting or crystallization differentiation. However, during subduction magmatism, the sediments are rich in Th and depleted in Ta. The addition of a small amount of sediment melt can lead to an increase in the Th content of the magma, and an increase in the Th/Yb value can reflect the contribution of sediment melt in the source region (Elliott et al., 1997; Class et al., 2000; Singer et al., 2007). In contrast, the Ta content is sensitive to subduction fluids. The covariant relationship between the Th/Yb and Ta/Yb values suggests that the components (including sediments and fluids) derived from subduction contributed to the generation of the Yushigou gabbros (Figure 10C).

Tectonic discrimination diagrams of the elemental distributions of Si, Al, and Ti in the clinopyroxene compositions provide a distinct classification of magma types (Beccaluva et al., 1989). In the clinopyroxene Si *versus* Al diagram (Figure 10D), the sample fell into and near the MORB field. However, in the clinopyroxene Ti *versus* Al^{IV} diagram (Figure 10E), the sample falls within the island arc tholeiite (IAT) field. Grimes et al. (2007) used U, Th, Hf, Y, and Yb (as a monitor for HREEs) to discriminate crystallized zircons from the MORB mantle from those formed in continental magmatic settings. During subduction, easily migrated incompatible elements (such as large ion lithophile elements, LREEs, and U) are separated from non-migrated high-field strength elements (such as Nb, Y, and HREEs). These easily migrated incompatible elements are mobilized by plate-derived fluids to increase the U/Yb value in the magma (Grimes et al., 2015). Zircons from the Yushigou gabbros were mostly within the 90% confidence interval of the MORB zircons, as presented in Figure 10F, although several overlapped with primitive magmatic arc zircons. This suggests that zircons from the Yushigou gabbro formed in a subduction-related environment.

Three explanations have been proposed for the tectonic evolution of the North Qilian orogenic belt. The first suggests that the ancient ocean was a part of the Proto-Tethys and that the tectonic evolution of the North Qilian orogenic belt can be regarded as a portion of the Tethyan tectonic domain (Wang and Liu, 1976). The second hypothesis proposes that the ancient ocean represented a limited extensional oceanic basin developed on the southern margin of the North China Craton. The continental margin rifted and expanded to form this basin, which then closed to form an orogenic belt (Feng and He, 1996; Xia et al., 1996; 1998). The final explanation emphasizes that the ancient ocean in the North Qilian orogenic belt was part of the Paleo-Asian Ocean (Zhang et al., 1997). After several years of discussion, most scholars agree with the second hypothesis (Feng and He, 1994; Qian et al., 2001; Du et al., 2006a; 2006b; 2007; Zhu and Du, 2007).

After the division of the Rodinia supercontinent, the Qilian Ocean opened and expanded as part of the Iapetus Ocean from approximately 710–520 Ma (Song et al., 2013b). Basic rocks with mid-ocean ridge or back-arc basin characteristics have been identified in the Yushigou area with ages ranging from 550 to 521 Ma (Xia et al., 1998; Shi et al., 2004; Hou et al., 2006). Initial ocean subduction and infant arc magmatism occurred from 520 to 490 Ma, which caused partial melting of the mantle wedge and formed infant arc basalts from 517 to 505 Ma (Song et al., 2013b). Wu et al. (2010) identified arc volcanic granites with an age of 512 Ma. Song et al. (2013a) reported that the magmatic zircon age of the Chaidanuo intrusion was 516 ± 4 Ma, recording the oldest arc magmatic activity in the North Qilian Orogenic Belt. A report on the Dachadaban boninite (505 Ma) also suggested a pre-arc environment related to the inner oceanic island arc in the North Qilian orogenic belt (Chen et al., 1995; Meng et al., 2010). This implies the formation of back-arc basins (Song et al., 2013b). The study from Hou et al. (2006) of isotope means indicated that the Yushigou ophiolite most likely formed in a mid-ocean ridge or mature back-arc basin. Combined with previous data and this study, the back-arc basin of the North Qilian orogenic belt may have evolved to a relatively mature stage from 519 to 495 Ma.

Conclusion

1) The zircon U-Pb chronology shows that the gabbro in the Yushigou ophiolite from the North Qilian orogenic belt was formed from 519 to 495 Ma as a product of Cambrian magmatism.
2) The gabbro in the Yushigou ophiolite in the North Qilian orogenic belt belongs to the tholeiite series and exhibits typical N-MORB geochemical characteristics. The source area features characteristics of mantle source materials, and 1%–3% of subduction materials were added. When clinopyroxene minerals were formed, the magma temperature ranged from 1,221.3°C to 1,376.6°C, and the pressure ranged from 4.5 to 15 kbar. The

origin of the rocks may include a high degree of partial melting in the spinel lherzolite source area.

3) Whole-rock geochemistry and mineral analysis of gabbro in the Yushigou ophiolite in the North Qilian belt show the dual characteristics of MORB and IAT, suggesting that it may have formed in a back-arc basin environment.

Data availability statement

The original contributions presented in the study are included in the article/Supplementary Material, further inquiries can be directed to the corresponding authors.

Author contributions

HT: Investigation, Conceptualization, Data Curation, Formal analysis, Visualization, Writing–Original Draft, Writing–Review and Editing. XL (2nd author): Investigation, Conceptualization, Formal analysis, Supervision, Writing–Original Draft, Writing–Review and Editing, Funding acquisition, Project administration. HW: Conceptualization, Formal analysis, Visualization, Supervision, Writing–Original Draft, Writing–Review and Editing. DL: Investigation, Conceptualization. XL (5th author): Investigation, Conceptualization, Formal analysis, Writing–Original Draft, Writing–Review and Editing, Funding acquisition, Project administration. QS: Investigation. ZL: Data Curation, Formal analysis. RH: Investigation, Conceptualization. QY: Investigation, Conceptualization.

Funding

This work was financially supported by the National Natural Science Foundation of China (92055208, 42203051), the Guangxi Science Innovation Base Construction Foundation (GuikeZY21195031), Guangxi Natural Science Foundation of China for Young Scholars (2022GXNSFBA035538), and the Fifth Bagui Scholar Innovation Project of Guangxi Province (to Xu Jifeng).

Acknowledgments

We would like to thank the editors and reviewers for their constructive comments, which improved the quality of this paper. We would also like to thank Zhang Zhiguo, Xiao Yao, QS Yujia, Zhang Yinhui, Yu Hongxia, and Liu Yizhi for their help with analyses and fieldwork.

Conflict of interest

The authors declare that the research was conducted in the absence of any commercial or financial relationships that could be construed as a potential conflict of interest.

Publisher's note

All claims expressed in this article are solely those of the authors and do not necessarily represent those of their affiliated organizations, or those of the publisher, the editors and the reviewers. Any product that may be evaluated in this article, or claim that may be made by its manufacturer, is not guaranteed or endorsed by the publisher.

Supplementary material

The Supplementary Material for this article can be found online at: https://www.frontiersin.org/articles/10.3389/feart.2023.1192997/full#supplementary-material

References

Aldanmaz, E., Pearce, J. A., Thirlwall, M. F., and Mitchell, J. G. (2000). Petrogenetic evolution of late Cenozoic, post-collision volcanism in Western Anatolia, Turkey. *J. Volcanol. Geotherm. Res.* 102, 67–95. doi:10.1016/s0377-0273(00)00182-7

Allegre, C. J., and Minster, J. F. (1978). Quantitative models of trace element behavior in magmatic processes. *Earth Planet. Sci. Lett.* 38, 1–25. doi:10.1016/0012-821x(78)90123-1

Annen, C., Blundy, J. D., and Sparks, R. S. J. (2006). The genesis of intermediate and silicic magmas in deep crustal hot zones. *J. Petrology* 47 (3), 505–539. doi:10.1093/petrology/egi084

Beccaluva, L., Macciotta, G., Piccardo, G. B., and Zeda, O. (1989). Clinopyroxene composition of ophiolite basalts as petrogenetic indicator. *Chem. Geol.* 77, 165–182. doi:10.1016/0009-2541(89)90073-9

Buhn, B., Pimentel, M. M., Matteini, M., and Dantas, E. (2009). High spatial resolution analysis of Pb and U isotopes for geochronology by laser ablation multi-collector inductively coupled plasma mass spectrometry (LA-MC-ICP-MS). *Ann. Braz. Acad. Sci.* 81, 99–114. doi:10.1590/s0001-37652009000100011

Chauvel, C., and Blichert-Toft, J. E. (2001). A hafnium isotope and trace element perspective on melting of the depleted mantle. *Earth Planet. Sci. Lett.* 190, 137–151. doi:10.1016/s0012-821x(01)00379-x

Chen, Y., Song, S., Niu, Y., and Wei, C. (2014). Melting of continental crust during subduction initiation: A case study from the Chaidanuo peraluminous granite in the North Qilian suture zone. *Geochimica Cosmochimica Acta* 132, 311–336. doi:10.1016/j.gca.2014.02.011

Chen, Y., Zhou, D. J., and Wang, E. Q. (1995). Discovery and geochemical characteristics of bothite series rocks in dacha daban ophiolite, sunan county, northern qilian. *Acta Petrol. Sin.* 11, 147–153. (in Chinese with English abstract).

Class, C., Miller, D. M., Goldstein, S. L., and Langmuir, C. H. (2000). Distinguishing melt and fluid subduction components in umnak volcanics, aleutian arc: DISTINGUISHING melt and fluid subduction components in umnak volcanics, aleutian ARCfluid subduction components in umnak volcanics, aleutian arc. *Geochem. Geophys. Geosystems* 1. doi:10.1029/1999gc000010

Coleman, R. G. (1977). Ophiolite: Ancient oceanic lithosphere? *Mineral. Mag.* 42 (322).

Condie, K. C. (1989). Geochemical changes in baslts and andesites across the archean-proterozoic boundary: Identification and significance. *Lithos* 23 (1-2), 1–18. doi:10.1016/0024-4937(89)90020-0

Corfu, F., Hanchar, J. M., Hoskin, P., and Kinny, P. (2003). Atlas of zircon textures. *Rev. Mineralogy Geochem.* 16, 469–500. doi:10.2113/0530469

Dilek, Y., and Furnes, H. (2011). Ophiolite Genesis and global tectonics: Geochemical and tectonic fingerprinting of ancient oceanic lithosphere. *Geol. Soc. Am. Bull.* 123 (3-4), 387–411. doi:10.1130/b30446.1

Dilek, Y., Furnes, H., and Shallo, M. (2007). Suprasubduction zone ophiolite formation along the periphery of Mesozoic Gondwana. *Gondwana Res.* 11 (4), 453–475. doi:10.1016/j.gr.2007.01.005

Dilek, Y. (2003). *Ophiolite concept and its evolution*, 373. Special Paper of the Geological Society of America, 1–16.

Du, Y. S., Zhu, J., and Gu, S. L. (2006b). Geochemical characteristics and tectonic significance of ordovician siliceous rocks in shihuigou, yongdeng, North Qilian. *Geol. Rev.* 52 (2), 184–189. (in Chinese with English abstract).

Du, Y. S., Zhu, J., and Gu, S. L. (2007). Sedimentary geochemical characteristics of Cambrian-Ordovician siliceous rocks in North Qilian orogenic belt and their enlightenment to multi-island oceans. *Chin. Sci. Ser. D Earth Sci.* 37 (10), 1314–1329. (in Chinese with English abstract).

Du, Y. S., Zhu, J., and Gu, S. L. (2006a). Sedimentary geochemical characteristics of Ordovician siliceous rocks in Sunan area of North Qilian Mountains and their tectonic significance of multi-island oceans. *Geosciences-Journal China Univ. Geosciences* 31 (1), 101–109. (in Chinese with English abstract).

Elliott, T., Plank, T., Zindler, A., White, W., and Bourdon, B. (1997). Element transport from slab to volcanic front at the Mariana arc. *J. Geophys. Res.* 102, 14991–15019. doi:10.1029/97jb00788

Elthon, D. (1987). Petrology of gabbroic rocks from the mid-cayman rise spreading center. *J. Geophys. Res.* 92, 658–682. doi:10.1029/jb092ib01p00658

Feng, Y. M., and He, S. P. (1996). *Geotectonics and orogenesis of qilian orogenic belt*. Beijing: Geological Publishing House, 37–70. (in Chinese with English abstract).

Feng, Y. M., and He, S. P. (1994). Petrochemical characteristics and formation environment of Cambrian-Ordovician siliceous rocks in North Qilian. *Geol. Sci. northwest China* 15 (1), 17–25. (in Chinese with English abstract).

Feng, Y. M., and He, S. P. (1995). Research for geology and geochemistry of several ophiolites in the North Qilian Mountains, China. *Geol. Rev.* 40, 252–264. (in Chinese with English abstract).

Fu, C. L., Yan, Z., Wang, Z. Q., Buckman, S., Aitchison, J. C., Niu, M., et al. (2018). Lajishankou ophiolite complex: Implications for paleozoic multiple accretionary and collisional events in the South Qilian belt. *Adv. Earth space Sci.* 37 (5), 1321–1346. doi:10.1029/2017tc004740

Griffin, W. L., Pearson, N. J., Belousova, E., Jackson, S., van Achterbergh, E., O'Reilly, S. Y., et al. (2000). The Hf isotope composition of cratonic mantle: LAM-MC-ICPMS analysis of zircon megacrysts in kimberlites. *Geochimica Cosmochimica Acta* 64, 133–147. doi:10.1016/s0016-7037(99)00343-9

Griffin, W. L., Wang, X., Jackson, S. E., Pearson, N., O'Reilly, S. Y., Xu, X., et al. (2002). Zircon chemistry and magma mixing, SE China: *In-situ* analysis of Hf isotopes, tonglu and pingtan igneous complexes. *Lithos* 61, 237–269. doi:10.1016/s0024-4937(02)00082-8

Grimes, C. B., John, B. E., Kelemen, P. B., Mazdab, F., Wooden, J. L., Cheadle, M. J., et al. (2007). Trace element chemistry of zircons from oceanic crust: A method for distinguishing detrital zircon provenance. *Geology* 35, 643–646. doi:10.1130/g23603a.1

Grimes, C. B., Wooden, J. L., Cheadle, M. J., and John, B. E. (2015). Fingerprinting" tectono-magmatic provenance using trace elements in igneous zircon. *Contributions Mineralogy Petrology* 170, 46. doi:10.1007/s00410-015-1199-3

Henstock, T., Woods, A., and White, R. (1993). The accretion of oceanic crust by episodic sill intrusion. *J. Geophys. Res.* 98, 4143–4161. doi:10.1029/92jb02661

Hou, Q. Y., Zhao, Z. D., Zhang, H. F., Zhang, B. R., and Chen, Y. L. (2006). Indian ocean-MORB-type isotopic signature of Yushigou ophiolite in North Qilian mountains and its implications. *Chin. Sci. Ser. D Earth Sci.* 49 (6), 561–572. doi:10.1007/s11430-006-0561-8

Kelemen, P., Koga, K., and Shimizu, N. (1997). Geochemistry of gabbro sills in the crust-mantle transition zone of the Oman ophiolite: Implications for the origin of the oceanic lower crust. *Earth Planet. Sci. Lett.* 146, 475–488. doi:10.1016/s0012-821x(96)00235-x

Kessel, R., Schmidt, W., Ulmer, P., and Pettke, T. (2005). Trace element signature of subduction-zone fluids, melts and supercritical liquids at 120–180 km depth. *Nature* 437 (7059), 724–727. doi:10.1038/nature03971

Kuritani, T., Ohtani, E., and Kimura, J. I. (2011). Intensive hydration of the mantle transition zone beneath China caused by ancient slab stagnation. *Nat. Geosci.* 4 (10), 713–716. doi:10.1038/ngeo1250

Le Bas, M. J. (1962). The role of aluminum in igneous clinopyroxenes with relation to their parentage. *Am. J. Sci.* 260, 267–288. doi:10.2475/ajs.260.4.267

Le Bas, M. J., Le Meaitre, R. W., Streckeisen, A., and Zanettin, B. (1986). A chemical classification of volcanic rocks based on the total alkali-silica diagram. *J. Petrology* 27 (3), 745–750. doi:10.1093/petrology/27.3.745

Le Roex, A. P., Dick, H. J. B., Erlank, A. J., Reid, A. M., Frey, F. A., and Hart, S. R. (1983). Geochemistry, mineralogy and petrogenesis of lavas erupted along the southwest Indian ridge between the bouvet triple junction and 11 degrees east. *J. Petrology* 24, 267–318. doi:10.1093/petrology/24.3.267

Lee, C.-T. A., Luffi, P., Plank, T., Dalton, H., and Leeman, W. P. (2009). Constraints on the depths and temperatures of basal-tic magma generation on Earth and other terrestrial planets using new thermobarometers for mafic magmas. *Earth Planet. Sci. Lett.* 279 (1-2), 20–33. doi:10.1016/j.epsl.2008.12.020

Li, C. Y., Liu, Y. W., Zhu, B. C., Feng, Y. M., and Wu, H. Q. (1978). "Structural evolutions of qinling and qilian," in *Scientific papers on Geology for international exchange* (Beijing: Editorial Office of Chinese Geological Bureau, Geological Publishing House, 174–189. (in Chinese with English abstract).

Lister, G., and Forster, M. (2009). Tectonic mode switches and the nature of orogenesis. *Lithos* 113 (1-2), 274–291. doi:10.1016/j.lithos.2008.10.024

Liu, X. J., Zhang, Z. G., Xu, J. F., Xiao, W. J., Shi, Y., Gong, X. H., et al. (2020). The youngest permian ocean in central asian orogenic belt: Evidence from geochronology and geochemistry of bingdaban ophiolitic melange in central tianshan, northwestern China. *Geol. J.* 55 (3), 2062–2079. doi:10.1002/gj.3698

Liu, Y. S., Hu, Z. C., Gao, S., Günther, D., Xu, J., et al. (2008). *In situ* analysis of major and trace elements of anhydrous minerals by LA- ICP-MS without applying an internal standard. *Chem. Geol.* 257 (1-2), 34–43. doi:10.1016/j.chemgeo.2008.08.004

Ludwig, K. R. (2012). *Isoplot 3.75: A geochronological toolkit for microsoft Excel*. Berkeley geochronology center special Publication, 5.

Mahoney, J. J., Frei, R., Tejada, M. L. G., Mo, X. X., Leat, P. T., and Nägler, T. F. (1998). Tracing the Indian ocean mantle domain through time: Isotopic results from old west Indian, east tethyan, and South pacific seafloor. *J. Petrology* 39, 1285–1306. doi:10.1093/petroj/39.7.1285

Matteini, M., Junges, S. L., Dantas, E. L., Pimentel, M. M., and Bühn, B. (2010). *In situ* zircon U-Pb and Lu-Hf isotope systematic on magmatic rocks: Insights on the crustal evolution of the Neoproterozoic Goiás Magmatic Arc, Brasília belt, Central Brazil. *Gondwana Res.* 17 (1), 1–12. doi:10.1016/j.gr.2009.05.008

Meng, F. C., Zhang, J. X., Guo, M. C., and Li, J. P. (2010). Mor-type and SSZ-type ophiolites from DachaDaban to the North Qilian ocean evolutionary constraints. *Acta Petrologica Mineralogica* 29 (5), 453–466. (in Chinese with English Abstract).

Montanini, A., Tribuzio, R., and Vernia, L. (2008). Petrogenesis of basalts and gabbros from an ancient continent–ocean transition (External Liguride ophiolites, Northern Italy). *Lithos* 101, 453–479. doi:10.1016/j.lithos.2007.09.007

Morris, J. D., and Ryan, J. G. (2003). "Subduction zone processes and implications for changing composition of the upper and lower mantle," in *Treatisse on geochemistry*. Editors H. D. Holland and K. K. Turekian (Oxford: Elsevier), 2, 451–470.

Mullen, E. D. (1983). $MnO/TiO_2/P_20_5$ a minor element discriminant for basaltic rocks of oceanic environments and its implications for petrogenesis. *Earth Planet. Sci. Lett.* 62, 53–62. doi:10.1016/0012-821x(83)90070-5

Murphy, D. T., Collerson, K. D., and Kamber, B. S. (2002). Lamproites from Gaussberg, Antarctica: Possible transition zone melts of Archaean subducted sediments. *J. Petrology* 43 (6), 981–1001. doi:10.1093/petrology/43.6.981

Neave, D, A., and Putirka, K. D. (2017). A new clinopyroxene-liquid barometer, and implications for magma storage pressures under Icelandic rift zones. *Am. Mineralogist* 102 (4), 777–794. doi:10.2138/am-2017-5968

Pearce, J. A. (1996). "A user's guide to basaltic discrimination diagrams," in *Trace element geochemistry of volcanic rocks: Applications for massive sulphide exploration*. Editor D. A. Wyman (Geological Association of Canada Short Course Notes), 12, 79–113.

Pearce, J. A. (2008). Geochemical fingerprinting of oceanic basalts with applications to ophiolite classification and the search for archean oceanic crust. *Lithos* 100, 14–48. doi:10.1016/j.lithos.2007.06.016

Pearce, J. A., and Stern, R. J. (2006). "Origin of back arc basin magmas: Trace element and isotope perspectives," in *Back Arc spreading systems: Geological, biological, chemical, and physical interactions*. Editors D. M. Christie, C. R. Fisher, S. M. Lee, and S. Givens (Washington, D. C: American Geophysical Union), 166, 63–86.

Pearce, J. A. (1982). *Trace element characteristics of lavas from destructive plate boundaries: Andesites, Orogenic Andesites and Related Rocks*. Geology, 528–548.

Pearce, N. J., Perkins, W. T., Westgate, J. A., Gorton, M. P., Jackson, S. E., Neal, C. R., et al. (1997). A compilation of new and published major and trace element data for NIST SRM 610 and NIST SRM 612 glass reference materials. *Geostand. Geoanalytical Res.* 21 (1), 115–144. doi:10.1111/j.1751-908x.1997.tb00538.x

Putirka, K. D. (2008). Thermometers and barometers for volcanic systems. *Rev. Mineralogy Geochem.* 69, 61–120. doi:10.2138/rmg.2008.69.3

Qian, Q., Zhang, Q., and Sun, X. M. (2001). Formation environment and mantle source characteristics of Jiuquan Basalts in Northern Qilian: Constraints of trace elements and Nd isotope Geochemistry. *Acta Petrol. Sin.* 17 (3), 385–394. (in Chinese with English Abstract).

Rao, W. X. (2015). *The study on the mineralization mechanism of Yushigou chromite deposit, Qilianshan belt*. Master's thesis. Lanzhou University. (in Chinese with English Abstract).

Rubatto, D. (2002). Zircon trace element geochemistry: Partitioning with garnet and the link between U-Pb ages and metamorphism. *Chem. Geol.* 184, 123–138. doi:10.1016/s0009-2541(01)00355-2

Saccani, E. (2015). A new method of discriminating different types of post-Archean ophiolitic basalts and their tectonic significance using Th-Nb and Ce-Dy-Yb systematics. *Geosci. Front.* 6 (4), 481–501. doi:10.1016/j.gsf.2014.03.006

Saccani, E., Allahyari, K., Beccaluva, L., and Bianchini, G. (2013). Geochemistry and petrology of the Kermanshah ophiolites (Iran): Implication for the interaction between

passive rifting, oceanic accretion, and OIB-type components in the Southern Neo-Tethys Ocean. *Gondwana Res.* 24, 392–411. doi:10.1016/j.gr.2012.10.009

Saccani, E., Principi, G., Garfagnoli, F., and Menna, F. (2008). Corsica ophiolites: Geochemistry and petrogenesis of basaltic and metabasaltic rocks. *Ofioliti* 33, 187–207.

Shi, R. D., Yang, J. S., and Wu, C. L. (2004). SHRIMP age evidence of Yushigou ophiolite formed in late sinian in North Qilian. *Acta Geol. Sin.* 78 (5), 649–657. (in Chinese with English abstract).

Singer, B. S., Jicha, B. R., Leeman, W. P., Rogers, N. W., Thirlwall, M. F., Ryan, J., et al. (2007). Along-strike trace element and isotopic variation in Aleutian Island arc basalt: Subduction melts sediments and dehydrates serpentine. *J. Geophys. Research-Solid Earth* 112, B06206. doi:10.1029/2006jb004897

Sláma, J., Koler, J., Condon, D. J., Crowley, J. L., Gerdes, A., Hanchar, J. M., et al. (2008). Plešovice zircon — a new natural reference material for U–Pb and Hf isotopic microanalysis. *Chem. Geol.* 249 (1-2), 1–35. doi:10.1016/j.chemgeo.2007.11.005

Song, S. G., Niu, Y. L., Li, S., Zhang, C., and Zhang, L. F. (2014). Continental orogenesis from ocean subduction, continent collision/subduction, to orogen collapse, and orogen recycling: The example of the North Qaidam UHPM belt, NW China. *Earth Sci. Rev.* 129, 59–84. doi:10.1016/j.earscirev.2013.11.010

Song, S. G., Niu, Y. L., Su, L., and Xia, X. H. (2013a). Tectonics of the North Qilian orogen, NW China. *Gondwana Res.* 23 (4), 1378–1401. doi:10.1016/j.gr.2012.02.004

Song, S. G., Wu, Z. Z., Yang, L. M., Su, L., Xia, X. H., Wang, C., et al. (2019). Ophiolite belts and evolution of the proto-tethys ocean in the qilian orogen. *Acta Petrol. Sin.* 35 (10), 2948–2970. (in Chinese with English abstract). doi:10.18654/1000-0569/2019.10.02

Song, S. G., Zhang, G. B., Zhang, C., Zhang, L. F., and Wei, J. C. (2013b). Dynamic processes of oceanic subduction and continental collision: Petrological constraints of high-pressure and ultrahigh-pressure metamorphic belts in the northern qilian-qaidam margin. *Chin. Sci. Bull.* 58 (23), 2240–2245. (in Chinese with English abstract).

Song, S., Su, L., Li, X. H., Zhang, G., Niu, Y., and Zhang, L. (2010). Tracing the 850 Ma continental flood basalts from a piece of subducted continental crust in the North Qaidam UHPM belt, NW China. *Precambrian Res.* 183, 805–816. doi:10.1016/j.precamres.2010.09.008

Song, S., Wang, M. M., Xu, X., Wang, C., Niu, Y., Allen, M. B., et al. (2015). Ophiolites in the Xing'an-Inner Mongolia accretionary belt of the CAOB: Implications for two cycles of seafloor spreading and accretionary orogenic events. *Tectonics* 34 (10), 2221–2248. doi:10.1002/2015tc003948

Song, Z. B., Li, W. Y., Li, H. K., Li, H. M., and Li, Y. Z. (2007). Isotopic age of shijuli gabbro in North Qilian mountain and its geological significance. *Acta Geosci. Sinaca* 28 (1), 7–10. (in Chinese with English abstract).

Sun, S., and McDonough, W. F. (1989). Chemical and isotopic systematics of oceanic basalts: Implications for mantle composition and processes. *Geol. Soc. Lond. Spec. Publ.* 42 (1), 313–345. doi:10.1144/gsl.sp.1989.042.01.19

Tseng, C. Y., Yang, H. J., Yang, H. Y., Liu, D. Y., Tsai, C. L., Wu, H. Q., et al. (2007). The dongcaohe ophiolite from the North Qilian mountains: A fossil oceanic crust of the paleo-qilian ocean. *Chin. Sci. Bull.* 52, 2390–2401. doi:10.1007/s11434-007-0300-3

Wang, Q., and Liu, X. (1976). Paleo-oceanic crust of the Chilienshan region, Western China and its tectonic significance. *Scinetia Geol. Sin.* (1), 42–55. (in Chinese with English abstract).

Williams, I. S. (2001). Response of detrital zircon and monazite, and their U-Pb isotopic systems, to regional metamorphism and host-rock partial melting, Cooma Complex, southeastern Australia. *J. Geol. Soc. Aust.* 48 (4), 557–580. doi:10.1046/j.1440-0952.2001.00883.x

Wu, C. L., Xu, X. Y., Gao, Q. M., Li, X. M., and Lei, M. (2010). Early Paleozoic granitic magmatism and tectonic evolution in Northern Qilian. *Acta Petrol. Sinca* 26 (04), 1027–1044. (in Chinese with English abstract).

Wu, H., Li, C., Yu, Y., and Chen, J. (2018). Age, origin, and geodynamic significance of high-Al plagiogranites in the Labuco area of central Tibet. *Lithosphere* 10 (2), 351–363. doi:10.1130/l711.1

Xia, L. Q., Xia, Z. C., and Xu, X. Y. (1995). Dynamics of tectonic-volcanic magma evolution in North Qilian mountains. *Northwest. Geol.* 1, 1–28. (in Chinese with English abstract).

Xia, L. Q., Xia, Z. C., and Xu, X. Y. (1996). *Petrogenesis on marine volcanic rocks in North Qilian mountains*. Beijing: Geological Publishing House, 5–146. (in Chinese with English abstract).

Xia, L. Q., Xia, Z. C., and Xu, X. Y. (1998). *Volcanism and mineralization in qilian orogenic belt and adjacent areas*. Beijing: Geological Publishing House, 4–55. (in Chinese with English abstract).

Xia, X. H., and Song, S. G. (2010). Forming age and tectono-petrogenises of the jiugequan ophiolite in the North Qilian mountain, NW China. *Chin. Sci. Bull.* 55 (18), 1899–1907. doi:10.1007/s11434-010-3207-3

Xia, X. H., Song, S. S., and Niu, Y. L. (2012). Tholeiite-Boninite terrane in the North Qilian suture zone: Implications for subduction initiation and back-arc basin development. *Chem. Geol.* 328, 259–277. doi:10.1016/j.chemgeo.2011.12.001

Xiang, Z. Q., Lu, S. N., Li, H. K., Li, H. M., Song, B., and Zheng, J. K. (2007). Zircon SHRIMP U-Pb age of Zhuoyougou gabbro in the Western part of North Qilian Mountains and its geological significance. *Geol. Bull. China* 26 (12), 1686–1691. (in Chinese with English abstract).

Xiao, L., Xu, Y. G., Mei, H. J., and Sha, S. L. (2003). Geochemical characteristics of emeishan basalt in binchuan area, yunnan Province: Rock types and evolution law with time. *Chin. J. Geol.* 4, 478–494. (in Chinese with English abstract).

Xiao, X. C., Chen, G. M., and Zhu, Z. Z. (1978). Geological tectonic significance of ancient ophiolite belt in Qilian Mountains. *Acta Geol. Sin.* 4, 281–295+338. (in Chinese with English abstract).

Yan, X. X. (2014). *Petrological chronological characteristics and tectonic significance of Yushigou ophiolite suite in Qinghai Province*. Beijing: China University of Geosciences. (in Chinese with English abstract).

Yan, Z., Fu, C. L., Aitchison, J. C., Niu, M. L., Buckman, S., and Cao, B. (2019). Early cambrian muli arc-ophiolite complex: A relic of the proto-tethys oceanic lithosphere in the qilian orogen, NW China. *Int. J. Earth Sci.* 108 (4), 1147–1164. doi:10.1007/s00531-019-01699-6

Yan, Z., Li, J. L., and Yong, Y. (2008). Tectonic environment for the formation of ordovician carbonate-siliceous rocks in shihuigou, North Qilian. *Acta Petrosinica Sin.* 24 (10), 2384–2394. (in Chinese with English abstract).

Yang, G. X., Li, Y. J., Tong, L. L., Wang, Z. P., Si, G. H., Lindagato, P., et al. (2022). Natural observations of subduction initiation: Implications for the geodynamic evolution of the Paleo-Asian Ocean. *Paleo-Asian Ocean. Geosystems Geoenvironment* 1 (1), 100009. doi:10.1016/j.geogeo.2021.10.004

Yang, H., and Gu, L. X. (1990). Petrogenetic significance of La/Sm-La covariant diagram. *J. Guilin Coll. Geol.* 2, 201–208. (in Chinese with English abstract).

Yang, J. S., Xu, Z. Q., Zhang, J. X., Chu, J. Y., Zhang, R. Y., and Liu, J. G. (2001). "Tectonic significance of caledonian high-pressure rocks in the qilian–qaidam–altun mountains, NW China," in *Paleozoic and mesozoic tectonic evolution of central asia: From continental assembly to intracontinental deformation*. Editors Marc S. Hendrix and Greg A. Davis (Geological Society of America, Memoir), 194, 151–170.

Yoder, H., and Tilley, C. E. (1962). Origin of basalt magmas: An experimental study of natural and synthetic rock systems. *J. Petrology* 3, 342–532. doi:10.1093/petrology/3.3.342

Zeng, J. Y., Yang, H. R., Yang, H. Y., Liu, D. Y., Cai, J. L., Wu, H. Q., et al. (2007). Dongcaohe ophiolite in North Qilian: An early paleozoic oceanic crust fragment. *Chin. Sci. Bull.* 52 (7), 825–835. (in Chinese with English abstract).

Zhang, Q., Chen, Y., Zhou, D. J., Qian, Q., Jia, X. Q., and Han, Q. (1998). Geochemical characteristics and Genesis of dacha osaka ophiolite in North Qilian. *Chin. Sci. Ser. D Earth Sci.* 1, 30–33. (in Chinese with English abstract).

Zhang, Q., Sun, X., and Zhou, D. (1997). The characteristics of North Qilian ophiolites, forming settings and their tectonic significance. *Advence Earth Sci.* 12 (4), 366–393. (in Chinese with English abstract).

Zhang, Z. G., Liu, L., Liu, X. J., Hu, R. G., Gong, X. H., Tang, Z. J., et al. (2019). Geochronology, geochemistry and geological significance of volcanic rocks from Hamutusi area in Western Junggar, Xinjiang. *J. Guilin Univ. Technol.* 39 (2), 258–269. (in Chinese with English abstract).

Zhu, J., and Du, Y. S. (2007). Geochemical characteristics and paleogeographic significance of Ordovician siliceous rocks in Laohushan, North Qilian orogenic belt. *J. Paleogeogr.* 9 (1), 69–76. (in Chinese with English abstract).